Monolithic atom interferometry

Johannes Fiedler,[1,*] Kim Lefmann,[2] Wolf von Klitzing,[3] and Bodil Holst[1,†]
[1]*Department of Physics and Technology, University of Bergen, Allégaten 55, 5007 Bergen, Norway*
[2]*Niels Bohr Institute, University of Copenhagen, Universitetsparken 5, 2100 København, Denmark*
[3]*Institute of Electronic Structure and Laser, Foundation for Research and Technology-Hellas, Heraklion 70013, Greece*

(Received 8 February 2023; revised 12 May 2023; accepted 7 July 2023; published 7 August 2023)

Atom and, more recently, molecule interferometers are used in fundamental research and industrial applications. Most atom interferometers rely on gratings made from laser beams, which can provide high precision, but cannot reach very short wavelengths and require complex laser systems to function. Contrary to this, simple monolithic interferometers cut from single crystals offer (sub) nanometer wavelengths with an extreme level of stability and robustness. Such devices were conceived and demonstrated several decades ago for neutrons and electrons. Here, we propose a monolithic design for a thermal-beam molecule interferometer based on (quantum) reflection. We show, as an example, how a reflective, monolithic interferometer (Mach-Zehnder type) can be realized for a helium beam using Si(111)-H(1 × 1) surfaces, which have previously been demonstrated to act as very robust and stable diffractive mirrors for neutral helium atoms.

DOI: 10.1103/PhysRevA.108.023306

I. INTRODUCTION

The field of atom interferometry has expanded enormously over the last few decades. Atom interferometers are used in various applications, from magnetic and gravity sensing [1,2], quantum metrology [3], to atomic clocks [4]. They may even be used as dark matter and gravitational wave detectors [5] also in space [6,7]. Compact, portable atom gravimeters for prospecting, oil survey, and geophysical investigations have recently become commercially available [8]. Atom interferometers will also be useful as accelerometers for subsea navigation in submarines, and more recently, underwater drones [2,9]. This, however, will require very compact solutions, which are not presently available.

Atom interferometers use either cold atoms (including Bose-Einstein condensates) [10] or thermal atoms beams [11], and more recently, hot thermal vapors [12]. Most optical interferometers have, by now, been realized as atom interferometers, including Young's double slit, Mach-Zehnder, Talbot-Lau, Ramsey-Bordé, and Sagnac interferometers.

Historically, Young's double slit makes the simplest atom interferometer. The beam is split into two paths by passing through a double slit and the interference pattern is observed on a screen further down the beam path. It was realized for atoms for the first time in 1991 using metastable helium atoms passing through a thin gold foil [13].

The simplest split-path atom interferometer is arguably the Mach-Zehnder interferometer. It exploits the de Broglie wavelength of the atoms in a diffraction grating configuration with split beam paths. The first Mach-Zehnder atom interferometer was realized in 1991 [11] using a sodium beam and solid transmission diffraction gratings. Later in 1995, it was developed further by using metastable neon and argon and transmission diffraction gratings made of standing light waves [14,15], in 2002 using ground-state lithium also with light-wave gratings [16] and later again using neutral helium with solid gratings. Results from the last-mentioned instrument were never published, but it was mentioned in a review paper from 2009 [17].

In the Talbot-Lau interferometer, the self-imaging property of a grating is exploited in near-field diffraction. The atom paths are not truly separated; therefore, this type of interferometer has been used extensively for experiments with heavy molecules where the de Broglie wavelength is very small. The first Talbot-Lau atom interferometer was realized in 1994 [18].

Where the Mach-Zehnder interferometer and the Talbot-Lau interferometers are adapted from light optics, the Ramsey-Bordé interferometer, first realized in 1949 by Ramsey [19], can only be used for atoms: the principle is diffraction by absorption of a single photon on a weakly allowed transition to split the wave package. In the 1980th, this interferometer was further developed by Bordé by using atomic recoil to create a beam splitter [20]. This interferometer type is currently the standard for high-precision measurements, such as atomic clocks.

In light optics, the Sagnac interferometer, also called ring interferometer, relies on a beamsplitter mirror to create two beams that travel equidistant paths in opposite directions through a ring structure guided by reflective mirrors. The two beams meet at the starting point, where they interfere and are made to exit the ring. The first atom interferometer using the Sagnac effect was realized in 1991 using a Ramsey-Bordé

*johannes.fiedler@uib.no
†Bodil.Holst@uib.no

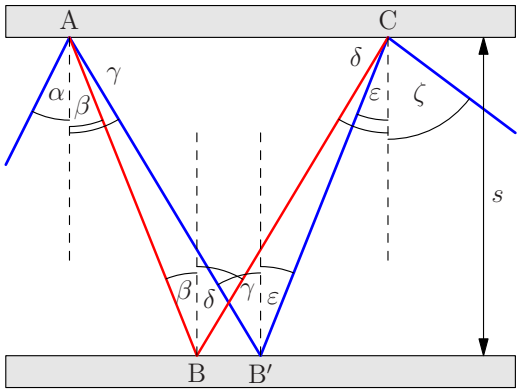

FIG. 1. Sketch of the optical paths within a monolithic, reflection interferometer: the beam is reflected three times between the surfaces of two parallel slabs (gray area) separated by the distance s. The incoming beam is reflected at point A with an incidence angle α. Two different diffraction orders are selected: Reflection towards point B with diffraction angle β and reflection towards B′ with diffraction angle γ. At point B, the incidence angle is the same as the outgoing angle in point A: β. Part of this beam is reflected towards point C with diffraction angle δ. At point B′, the incidence angle is given by γ due to the reflection at point A and reflected at the diffraction angle ε. In point C, the incoming waves with incidence angles δ and ε are recombined, leaving the slab with a reflection angle ζ

configuration of a state-labeled atom interferometer based on single-photon transitions, with a beam of atoms traversing two pairs of traveling wave fields. The laser fields within each pair are separated by a distance D, while the two pairs are separated by d and are counterpropagating with respect to each other [21]. By rotating the interferometer, the counterpropagating beams collect different phases along their optical paths leading to an interference pattern on the screen. Such a configuration provides an absolute measurement of the rotational speed.

The atomic structure of a single crystal offers a simple periodic diffractive grating. Thus, it could produce many different types of interferometers, where the monolithic construction guarantees extreme stability. Interferometers based on transmission through solid slabs of material have been demonstrated, e.g., x-rays [22,23], neutrons [24], and electrons [25]. Unfortunately, these techniques are inapplicable to atoms, which interact too strongly with any solid material they travel through. Monolithic atom interferometers have been used widely in neutron scattering experiments observing gravitationally induced interference (in transmission) [26] and the quantised states of neutrons in the presence of gravitational fields with perfectly reflecting mirrors [27]. Neutrons are sensitive to external forces, and thus, are suitable candidates for quantum sensing. However, such experiments require an extensive, costly infrastructure to create, control, and detect the neutron beam. This also applies to cold atom interferometers. Thermal atom beams are easier to create and couple more robust to external fields due to the higher mass of the atoms. A further advantage of thermal atom interferometers is that they can operate continuously, dramatically decreasing the temporal resolutions.

Here, we propose an interferometer based on the reflection of atoms on monolithic single-crystal structures. The basic operation principle is depicted in Fig. 1: an incident beam of atoms is reflected by the crystal lattice (A) into two components, which impinge onto a second mirror and recombine on the third reflection.

In the past, atoms had been neglected largely because the atoms most commonly used in interferometry (Rb [28]; Cs [29]; Ar [30]; Na [11]; K [18]) will stick to surfaces under most conditions. Similarly, metastable atoms, which have also been used for interferometry (Ar [31]; He [13]), will decay upon impingement. A further practical challenge for a reflection-based interferometer is the contamination of the reflecting surface, which distorts the diffraction. For example, all metal surfaces will be covered in physisorbed molecules within hours, even in an ultrahigh vacuum [32–34].

Noble gasses, including ground-state helium, H_2, HCl, and other molecules are known to scatter from various surfaces over a broad temperature range without sticking to them [35–37]. Over the last years, focusing mirrors for neutral, ground-state helium have been developed for neutral helium microscopes [38]. An important requirement for these mirrors is that they must remain stable in a vacuum for months. One of the solutions implemented was Si(111)-H(1 × 1) [39]. Detailed experiments on He and H_2 scattering were performed [40,41] and the interaction potential between helium and Si(111)-H(1 × 1) calculated [41]. This interaction potential was then used to obtain the intensity of the different diffraction peaks for a range of conditions [42].

The advantage of the Si(111)-H(1 × 1) surface from an experimental point of view is that it can be prepared chemically by dipping the Si(111) crystal in an HF solution [43]. This means a monolithic configuration with two reflecting surfaces facing each other can be fabricated at any spacing. The additional advantage of using the Si(111)-H(1 × 1) surface is the small lattice constant of $a_S = 3.383$ Å [40], which, together with the wavelength of, as an example, helium atoms in a room temperature beam $\lambda_{dB} = 0.55$ Å, ensures a very big wave-package separation. Recent matter-wave interferometers typically split the wave package over a few milliradian [31,44–46]. In contrast, using the room-temperature helium beam described above, the proposed interferometer splits the matter wave over 0.5 radians.

The atom interferometer we introduce here uses reflective atom-surface diffraction as a beam splitter. Further reflections from a parallel surface yield the recombination of the wave and thus the interference; see Fig. 1. We present a theoretical model determining the expected interference patterns and apply the model to the interference of helium atoms using Si(111)-H(1 × 1) surfaces, where we concentrate on describing the general principles by describing an ideal system with a perfectly coherent and monochromatic beam and an experimentally based model for the diffraction probabilities. We chose an experimentally realizable parameter set providing all possible superpositions occurring in such an interferometer: single-path transmission, double-path superposition with vanishing phases, and multipath interference. Finally, we discuss how a reflective interferometer based on quantum reflection

can be addressed. The paper finishes with a conclusion and outlook on future work.

II. REFLECTIVE INTERFEROMETER

A. Geometric arrangement

The general arrangement of a monolithic reflection interferometer is depicted in Fig. 1. A slab is cut into a U-shaped monolith to form two parallel planar surfaces with a distance s being sufficiently large to achieve propagating waves inside the interferometer. A particle beam will be diffracted minimally three times at points A, B, and C. The beam will be split at point A, and each part will be reflected at point B and recombined in point C, where they interfere.

In more detail, a particle beam is sent via an incidence angle α towards one surface. It is reflectively split in point A into a range of diffraction orders determined by the incident beam angle α, the periodic surface structure described by the lattice spacing a_S, and the beam wavelength λ through the well-known reciprocal lattice equation [47]. We pick two orders, the first one with the reflection angle β

$$\sin\beta = \sin\alpha + \frac{n_1\lambda}{a_S}, \tag{1}$$

with an integer $n_i \in \mathbb{Z}$ (numerating the diffraction order) and the second one with reflection angle γ

$$\sin\gamma = \sin\alpha + \frac{n_{1'}\lambda}{a_S}. \tag{2}$$

At point A, the two selected diffraction orders propagate towards points B and B′, where they are reflected towards point C and recombine. Point B denotes the reflection point one diffraction order from point A; thus, the corresponding incidence angle is β. To satisfy the recombination of the beam, the reflection angle δ has to be of a nonzeroth diffraction order expressed as

$$\sin\delta = \sin\beta + \frac{n_2\lambda}{a_S} = \sin\alpha + \frac{(n_1+n_2)\lambda}{a_S}. \tag{3}$$

Analogously, the reflection at point B′ can be determined by

$$\sin\varepsilon = \sin\gamma + \frac{n_{2'}\lambda}{a_S} = \cos\alpha + \frac{(n_{1'}+n_{2'})\lambda}{a_S}. \tag{4}$$

To satisfy the recombination of the beam at point C, the diffraction of the incoming beams need to occur under the same diffraction angle, which can be described mathematically by the relation

$$\sin\zeta = \sin\delta + \frac{n_3\lambda}{a_S} = \sin\alpha + \frac{(n_1+n_2+n_3)\lambda}{a_S}, \tag{5}$$

and

$$\sin\zeta = \sin\varepsilon + \frac{n_{3'}\lambda}{a_S} = \sin\alpha + \frac{(n_{1'}+n_{2'}+n_{3'})\lambda}{a_S}. \tag{6}$$

These equations yield a constrain for the diffraction orders

$$n_{3'} = n_1 + n_2 + n_3 - n_{1'} - n_{2'}. \tag{7}$$

In addition to this angular dependence, the distance between points A and C needs to be the same for both paths to satisfy the recombination of the beams. Figure 1 illustrates this condition: the blue and red beamlines need to recombine in the same point C. Otherwise, they would be reflected without any spatial overlap to interfere directly. If they are reflected into parallel beams from different spots, they will interfere in the far field with a phase shift proportional to the spatial difference between both points. To achieve interference also in the optical near-field regime for the entire interferometer, the condition reads

$$\tan\beta + \tan\delta = \tan\gamma + \tan\varepsilon. \tag{8}$$

Finally, we sum up six parameters characterizing a reflective atom interferometer which have to satisfy the conditions (7) and (8). These conditions can either be used for determining the incidence angle α or by rewriting the equation

$$\begin{aligned}&\tan(c+N_1) + \tan(c+N_1+N_2)\\ &\quad - \tan(c+N_{1'}) - \tan(c+N_{1'}+N_{2'}) = 0,\end{aligned} \tag{9}$$

with $c = \cos\alpha$ and $N_i = n_i\lambda/a_S$; one finds the following conditions leading to an α-independent solution:

$$n_1 = n_{1'} + n_{2'} \wedge n_{1'} = n_1 + n_2. \tag{10}$$

The interference pattern is due to the phase shift along the different optical paths ABC and AB′C. The path lengths can be determined via these angles for the path along point B

$$b = s\left(\frac{1}{\cos\beta} + \frac{1}{\cos\delta}\right), \tag{11}$$

and along the point B′

$$b' = s\left(\frac{1}{\cos\gamma} + \frac{1}{\cos\varepsilon}\right). \tag{12}$$

The interference occurs via the superposition of two waves with the same wave vector $\boldsymbol{k}$, but are phase shifted with respect to the respective path lengths $b - b'$. Hence, the phase shifts between the different paths are given by

$$\varphi = k(b - b'). \tag{13}$$

It can be observed in Eqs. (11) and (12) that the path lengths are proportional to the slab separation s and, thus, s should be tuned with respect to the wave vector to maximize the phase shift between both interfering beams.

Figure 2 illustrates the positions of the different diffraction for different incidence angles α for a particular interferometer configuration. It can be seen that the diffraction orders are strongly separated. All lines are discontinued due to the finite length of the interferometer, which leads to some beams escaping the interferometer. These particles will likely hit the surface and fall into the interferometer; thus, they will not affect the interference patterns.

B. Reflection coefficients for the different beam paths inside the interferometer

In the last section, the conditions for interference were obtained. We now consider the intensity distribution in the

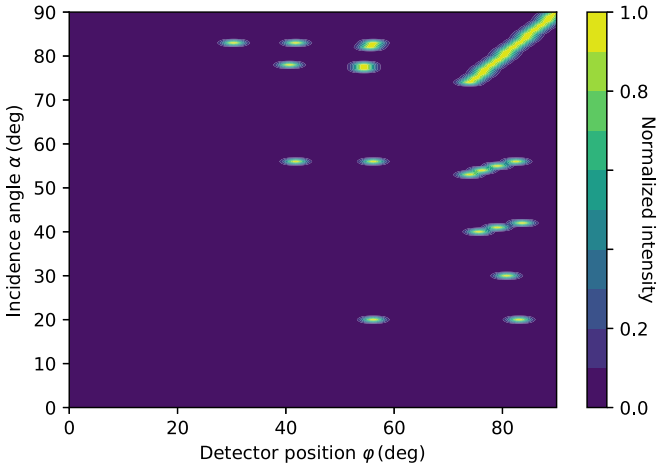

FIG. 2. Distribution of the diffraction orders on the screen φ depending on the incidence angle α for a monolithic atom interferometer built of silicon with hydrogen-passivized surfaces, which are separated by 5 mm and have an extension of 50 mm. The considered wavelength was $\lambda = 0.55$ Å. The purple area describes the dark regions where no particle will appear. For each incidence angle α, the maximum population of the diffraction order is marked in yellow. The remaining peak intensities are plotted relative to the maximum intensity according to the color scale.

interference signal, described via a reflection function. This reflection function depends on the incidence and diffraction angle ϑ_1 and ϑ_2, respectively. We model the reflected beam via a Gaussian intensity distribution. Consequently, each diffraction order has a Gaussian profile which we normalize to the real-valued probability of each diffraction order ρ_n

$$r(\vartheta_1, \vartheta_2) = \sum_n \rho_n e^{-\frac{(\vartheta_2-\theta_n)^2}{2\sigma_n^2}}, \tag{14}$$

with the width of the diffracted signal σ_n and the position of the diffracted beam θ_n determined by Eq. (1). The widths depend on the incidence angle and wavelength $\sigma_n = \sigma_n(\lambda, \vartheta_1)$. These impacts are negligible for surface diffraction, the paper's content, due to the overall weak reflection signal [41]. The reflection coefficient (14) only includes the inelastic scattering, that the wavelength of the outgoing wave is the same as that of the incoming wave $\lambda_{\text{inc}} = \lambda_{\text{out}}$. Thus, the total reflected signal is smaller than 1, $\int d\vartheta_2\, r(\vartheta_1, \vartheta_2) < 1$.

In general, there are five lengths involved in such an interferometer: the wavelength (λ_{dB}), the dimensions of the interferometer (length d and slap separation s), and the free-space propagation lengths (source to interferometer L_1 and interferometer to detector L_2). Typically, these dimensions are on different length scales $\lambda_{\text{dB}} \ll d, s < L_1, L_2$. This consideration allows for the separation of length scales. Consequently, each particle will only interfere with itself inside the same optical path in the interferometer. Thus, we can treat each path inside the interferometer separately, and the collected diffraction image will follow from the Gaussian beam envelope. The partial waves will experience a different phase shift due to the optical path (13). Thus, we can describe the reflection properties of the entire *inter*ferometer with a single modified

TABLE I. Overview of beams expected from an 83° incidence angle reflected into the diffraction angle φ with the diffraction orders n_1, n_2, and n_3 with the first diffraction angle β in radians. The last columns describe the optical path length b and amplitudes a being the ratio of transmitted atoms into each diffraction channel (%).

Angle φ (deg)	n_1	$\beta(n_1)$	n_2	n_3	Path b (cm)	Ampl. a (%)
30.32	0	1.4486	−1	−2	5.00	0.0270
41.87	−1	0.9791	1	−2	5.00	0.0135
41.87	0	1.4486	−1	−1	5.00	0.0540
56.10	−2	0.7307	2	−1	4.77	0.0068
56.10	0	1.4486	−2	1	4.77	0.0270
56.10	−1	0.9791	1	−1	5.00	0.0270
56.10	0	1.4486	−1	0	5.00	0.1080
83.00	−2	0.7307	1	1	1.57	0.0135
83.00	−2	0.7307	2	0	4.77	0.0135
83.00	0	1.4486	−2	2	4.77	0.0135
83.00	−1	0.9791	0	1	1.79	0.0540
83.00	−1	0.9791	1	0	5.00	0.0540
83.00	0	1.4486	−1	1	5.00	0.0540
83.00	−1	0.9791	−1	2	1.57	0.0135

reflection coefficient

$$r_{\text{inter}}(\vartheta_1, \vartheta_2) = \sum_{n_1 n_2 n_3} \rho_{n_1}\rho_{n_2}\rho_{n_3} f_{n_1 n_2 n_3} e^{ikb_{n_1 n_2}} e^{-\frac{[\vartheta_2 - \theta_{n_1 n_2 n_3}(\vartheta_1)]^2}{2\sigma^2}}, \tag{15}$$

with the wave vector of the matter wave $k = 2\pi/\lambda$ and the indicator function $f_{n_1 n_2 n_3}$ factoring in the interferometer's geometry (which determines whether the beam can pass through the interferometer or not). The beam spread of all diffraction orders will usually be the same for a monochromatic wave, $\sigma = \sigma_n$ for all diffraction orders n. Due to the tilted reflective surfaces with respect to the beam incidence, the detected spots will be slightly asymmetric, which we neglect for consideration in this paper. The position of the diffraction order is given by $\theta_{n_1 n_2 n_3}(\vartheta_1)$, which is the three-times composition of Eq. (1) simplifying to

$$\theta_{n_1 n_2 n_3}(\vartheta_1) = \arcsin\left[\sin\vartheta_1 + \frac{(n_1 + n_2 + n_3)\lambda}{a_{\text{S}}}\right]. \tag{16}$$

C. Monolithic interferometer for He and Si(111)-H(1 × 1)

Let us consider a helium beam with de Broglie wavelength $\lambda_{\text{dB}} = 0.55$ Å and a beam spread of 1 mrad at a distance of 1 m from the interferometer (propagation length $L_1 = 1$ m). This corresponds to a 1-mm beam waist ($w = 1$ mm) as the beam enters the interferometer. The lattice spacing of Si(111)-H(1 × 1) is $a_{\text{S}} = 3.383$ Å [40]. We consider an incidence angle of 83° and the reflection coefficient (14) with the amplitudes $\rho_0 = 0.06$, $\rho_{\pm1} = 0.03$, and $\rho_{\pm2} = 0.015$. These scattering values correspond to the experimentally obtained data for a beam with a wavelength of 0.6 Å and an incidence angle of 52° reported in Ref. [40]. We changed the incidence angle because the result would be restricted to the zeroth order; see Fig. 2. Table I shows the ratio of transmitted atoms into each diffraction channel. The reflection coefficients influence only the amplitude of the interference patterns, not

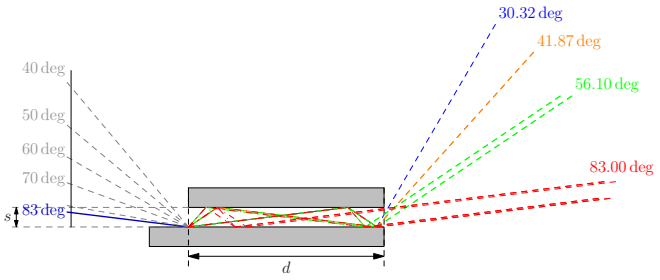

FIG. 3. Optical paths in a monolithic reflective atom interferometer: a slab cut into a monolithic crystal of length d (50 mm) and width s (5 mm). A helium beam with an incidence angle of 83° (dark blue line) enters the interferometer. It is diffracted at the hydrogen-passivized surfaces with a lattice constant $a_S = 3.383$ Å. The diffracted orders are reflected two more times until they leave the interferometer. It can be seen that the third-order ($-3 = n_1 + n_2 + n_3$) diffraction beam will not show any interference (blue dashed line at 30.32°), see Table I, the second-order beam at 41.87° (orange lines) will not show any interference due to equal optical path lengths; the diffraction at 56.10° (green lines), the zeroth order at 83.00° (red lines) will be measured separately in the near-field regime, whereas they will interfere in the far-field leading to the interference patterns depicted in Fig. 4.

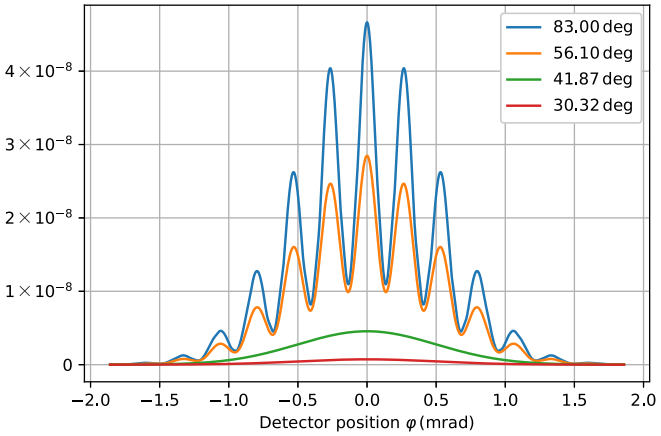

FIG. 4. Far-field diffraction patterns of each spot at 30.32° (red lower line), 41.87° (green line), 56.10° (orange line), and 83.00° (blue upper line) for a helium beam with wavelength $\lambda_{dB} = 0.55$ Å with an incidence angle of 83°.

the position of the peaks. Thus, the impact of the correct scattering amplitudes is insignificant. We chose the parameters to demonstrate several effects: the single-beam transmission, the two-path superposition, and the multipath interference. Here we restrict our considerations to the zeroth, first, and second diffraction orders. Furthermore, we consider the reflecting plates to be 50-mm long and 5-mm separated from each other. The optical paths for this scenario are depicted in Fig. 3. It can be seen that the third-order diffraction beam (at 30.32°, blue line) consists of a single beam. It thus will not show any interference; the second-order beam (at 41.87°, orange line) is the superposition of two paths, as described in Sec. II A, but with equal optical paths which again will not interfere; and the first and zeroth order will show two separate signals each that will lead to interference in the far field. Due to the separation of the length scales and the fact that the atoms interfere with themselves and not with each other, we describe each interference pattern via a phase-shifted Gaussian wave in analogy to the Michelson interferometer. Thus, the interference pattern is described by the superposition of phase-shifted Gaussian waves

$$I(\varphi) \propto \left| \sum_n a_n e^{i\frac{k\sin\varphi}{2} b_n} \right|^2 e^{-\frac{2L_2^2 \sin^2\varphi}{w^2}}, \tag{17}$$

with the amplitudes $a_n = \rho_{n_1}\rho_{n_2}\rho_{n_3}$ and the optical path lengths b_n, which are given in Table I. The widths of the diffraction orders σ are small compared to the width of the Gaussian envelope $L_2 \sin\sigma \ll w$, and, hence, can be neglected. It can be seen in Eq. (17) that the interference fringes are determined by the wave vector $k = 2\pi/\lambda_{dB}$. Thus, increasing the wavelength, either by increasing the particle's mass or velocity will reduce the spacing between the interference fringes. The resulting interference patterns are plotted in Fig. 4. One can see that the diffraction at 30.32° and 41.87° will not show any interference features due to the equal optical path lengths of both optical paths. The remaining two spots will show interference effects with a contrast of 48.5% for the spot at 56.10° and 84.1% for the spot at 83.00°. The transmission rates of all channels can be found in Table I: 0.027% of the atoms will be diffracted under the angle of 30.32°, 0.0675% under 41.87°, 0.1688% under 56.10°, and 0.216% under 83°. The remaining particles will not leave the interferometer. The intensity of a typical helium beam is so big [48] that a signal fraction of 10^{-4} can easily be detected. The velocity spread will be the limiting quantity to measure the interference patterns for the helium atom interferometry configuration depicted in Fig. 4. The velocity spread of a supersonic helium beam depends on the beam temperature, the nozzle diameter, and the reservoir pressure. This has been treated extensively in the literature; see, for example, Ref. [49]. A velocity spread causes two different effects: (i) a broadening of the interference fringes and (ii) a spatial movement of the entire interference pattern, as illustrated in Fig. 5. Finally, to observe interference, the velocity spread has to be sufficiently small to not cause a washing out of the interference fringes. Figure 5 illustrates the positions of the diffraction order for different wavelengths of the incoming beam with a fixed incidence angle of 83°. It can be observed that the zeroth order will stay constant. The remaining orders strongly spread out with increasing wavelength. As in Fig. 2, the lines are not continuous due to the finite size of the interferometer. It can be seen in Table I that the interferometer splits the wave package at the first diffraction point over ≈0.71 rad.

D. Quantum reflection interferometer

Quantum reflection occurs on the attractive (outer) part of the atom-surface interaction potential [50] in contrast to surface scattering, where the reflection occurs on the repulsive (inner) part of the interaction potential [51,52]. It is called quantum reflection because, classically, reflection cannot occur with an attractive force interaction potential. Quantum reflection has the very big advantage that an extensive range

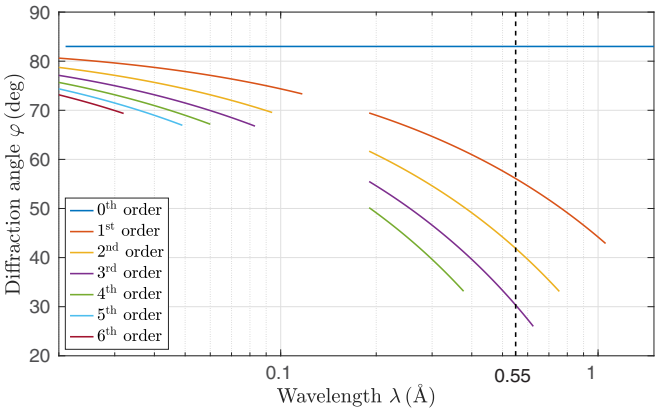

FIG. 5. Positions of the diffraction orders [from top to bottom: zeroth (blue); first (orange); second (yellow); third (purple); fourth (green); fifth (light blue); sixth (dark red)] for an incidence angle of 83° depending on the wavelength of the helium beam. The vertical black dashed line marks the regime for the considered scenario.

of atoms and small, few-atomic molecules that would stick under surface diffraction conditions display quantum reflection. The disadvantage is that quantum reflection requires small perpendicular wave vectors. This means that, for a given wavelength, the spatial extension of a reflective interferometer must be larger than in the surface scattering configuration for the separated beams to recombine.

Quantum reflection is less sensitive than surface scattering to defects and surface contamination because it occurs at larger distances from the surface [53]. Very large specular reflection coefficients of the order of 50% [54] up to 90% [55] have been measured. Diffraction via quantum reflection was recently demonstrated experimentally [56] using helium dimers and trimers with periodically striped surfaces with micron-sized structures. The paper includes a comparison of the experimental result with scattering theory based on the diffraction angle distribution (1), reported in Ref. [57]. There is reasonable agreement between theory and experiment.

III. CONCLUSION AND FUTURE WORK

This paper presents the first proposal for a reflective interferometer for atoms and molecules. We present calculations for a monolithic configuration based on experimental scattering results for a room-temperature helium beam from Si(111)-H(1 × 1), showing that a beam splitting of more than 0.5 radians is achievable. Furthermore, we argue that quantum reflection diffraction is a viable option for extending the beams and surfaces that can be used and potentially increase the signal intensity. The interference of larger and complex molecules can be achieved by using different interaction potentials, such as evanescent fields [51]. A reflective atom or molecule interferometer, particularly in a monolithic configuration, opens several possibilities for applications, for instance, as an accelerometer, in investigating the coherence of matters near dielectric surfaces, as a continuous velocity selector, and so on. The next obvious first step is to do a demonstration experiment of the interferometer with a helium beam and to do detailed designs of quantum reflection setups. This last will require the calculation of quantum (diffraction) reflection coefficients for a range of realistic system configurations.

ACKNOWLEDGMENTS

J.F. gratefully acknowledges support from the European Union (H2020-MSCA-IF-2020, Grant No. 101031712).

[1] B. Stray, A. Lamb, A. Kaushik, J. Vovrosh, A. Rodgers, J. Winch, F. Hayati, D. Boddice, A. Stabrawa, A. Niggebaum *et al.*, Quantum sensing for gravity cartography, Nature (London) **602**, 590 (2022).

[2] K. S. Hardman, P. J. Everitt, G. D. McDonald, P. Manju, P. B. Wigley, M. A. Sooriyabandara, C. C. N. Kuhn, J. E. Debs, J. D. Close, and N. P. Robins, Simultaneous Precision Gravimetry and Magnetic Gradiometry with a Bose-Einstein Condensate: A High Precision, Quantum Sensor, Phys. Rev. Lett. **117**, 138501 (2016).

[3] M. F. Riedel, P. Böhi, Y. Li, T. W. Hänsch, A. Sinatra, and P. Treutlein, Atom-chip-based generation of entanglement for quantum metrology, Nature (London) **464**, 1170 (2010).

[4] A. D. Ludlow, M. M. Boyd, J. Ye, E. Peik, and P. O. Schmidt, Optical atomic clocks, Rev. Mod. Phys. **87**, 637 (2015).

[5] B. Canuel, S. Abend, P. Amaro-Seoane, F. Badaracco, Q. Beaufils, A. Bertoldi, K. Bongs, P. Bouyer, C. Braxmaier, W. Chaibi *et al.*, ELGAR—a European laboratory for gravitation and atom-interferometric research, Class. Quantum Grav. **37**, 225017 (2020).

[6] Y. A. El-Neaj, C. Alpigiani, S. Amairi-Pyka, H. Araújo, A. Balaž, A. Bassi, L. Bathe-Peters, B. Battelier, A. Belić, E. Bentine *et al.*, Aedge - atomic experiment for dark matter and gravity exploration in space, EPJ Quantum Technology **7**, 6 (2020).

[7] G. M. Tino *et al.*, Precision gravity tests with atom interferometry in space, Nucl. Phys. B **243-244**, 203 (2013).

[8] V. Menoret, P. Vermeulen, N. L. Mogine, S. Bonvalot, P. Bouyer, A. Landragin, and B. Desruelle, Gravity measurements below $10^{-9}g$ with a transportable absolute quantum gravimeter, Sci. Rep. **8**, 12300 (2018).

[9] J. González-García, A. Gómez-Espinosa, E. Cuan-Urquizo, L. G. García-Valdovinos, T. Salgado-Jiménez, and J. A. E. Cabello, Autonomous underwater vehicles: Localization, navigation, and communication for collaborative missions, Appl. Sci. **10**, 1256 (2020).

[10] D. S. Hall, M. R. Matthews, C. E. Wieman, and E. A. Cornell, Measurements of Relative Phase in Two-Component Bose-Einstein Condensates, Phys. Rev. Lett. **81**, 1543 (1998).

[11] D. W. Keith, C. R. Ekstrom, Q. A. Turchette, and D. E. Pritchard, An Interferometer for Atoms, Phys. Rev. Lett. **66**, 2693 (1991).

[12] G. W. Biedermann, H. J. McGuinness, A. V. Rakholia, Y.-Y. Jau, D. R. Wheeler, J. D. Sterk, and G. R. Burns, Atom Interferometry in a Warm Vapor, Phys. Rev. Lett. **118**, 163601 (2017).

[13] O. Carnal, A. Faulstich, and J. Mlynek, Diffraction of metastable helium atoms by a transmission grating, Appl. Phys. B **53**, 88 (1991).

[14] D. M. Giltner, R. W. McGowan, and S. A. Lee, Atom Interferometer Based on Bragg Scattering from Standing Light Waves, Phys. Rev. Lett. **75**, 2638 (1995).

[15] E. M. Rasel, M. K. Oberthaler, H. Batelaan, J. Schmiedmayer, and A. Zeilinger, Atom Wave Interferometry with Diffraction Gratings of Light, Phys. Rev. Lett. **75**, 2633 (1995).

[16] R. Delhuille, C. Champenois, M. Büchner, L. Jozefowski, C. Rizzo, G. Trénec, and J. Vigué, High-contrast Mach–Zehnder lithium-atom interferometer in the Bragg regime, Appl. Phys. B **74**, 489 (2002).

[17] A. D. Cronin, J. Schmiedmayer, and D. E. Pritchard, Optics and interferometry with atoms and molecules, Rev. Mod. Phys. **81**, 1051 (2009).

[18] J. F. Clauser and S. Li, Talbov-vonlau atom interferometry with cold slow potassium, Phys. Rev. A **49**, R2213 (1994).

[19] N. F. Ramsey, A molecular beam resonance method with separated oscillating fields, Phys. Rev. **78**, 695 (1950).

[20] C. J. Bordé, Ch. Salomon, S. Avrillier, A. van Lerberghe, Ch. Bréant, D. Bassi, and G. Scoles, Optical Ramsey fringes with traveling waves, Phys. Rev. A **30**, 1836 (1984).

[21] F. Riehle, T. Kisters, A. Witte, J. Helmcke, and C. J. Bordé, Optical Ramsey Spectroscopy in a Rotating Frame: Sagnac Effect in a Matter-Wave Interferometer, Phys. Rev. Lett. **67**, 177 (1991).

[22] U. Bonse and M. Hart, An x-ray interferometer, Appl. Phys. Lett. **6**, 155 (1965).

[23] D. G. Chetwynd, S. C. Cockerton, S. T. Smith, and W. W. Fung, The design and operation of monolithic X-ray interferometers for super-precision metrology, Nanotechnology **2**, 1 (1991).

[24] H. Rauch and S. A. Werner, *Neutron Interferometry* (Oxford University Press, New York, 2015).

[25] A. Agarwal, C.-S. Kim, R. Hobbs, D. van Dyck, and K. K. Berggren, A nanofabricated, monolithic, path-separated electron interferometer, Sci. Rep. **7**, 1677 (2017).

[26] R. Colella, A. W. Overhauser, and S. A. Werner, Observation of Gravitationally Induced Quantum Interference, Phys. Rev. Lett. **34**, 1472 (1975).

[27] V. V. Nesvizhevsky, H. G. Börner, A. K. Petukhov, H. Abele, S. Baeßler, F. J. Rueß, T. Stöferle, A. Westphal, A. M. Gagarski, G. A. Petrov, and A. V. Strelkov, Quantum states of neutrons in the Earth's gravitational field, Nature (London) **415**, 297 (2002).

[28] L. Zhou, S. Long, B. Tang, X. Chen, F. Gao, W. Peng, W. Duan, J. Zhong, Z. Xiong, J. Wang, Y. Zhang, and M. Zhan, Test of Equivalence Principle at 10^{-8} Level By a Dual-Species Double-Diffraction Raman Atom Interferometer, Phys. Rev. Lett. **115**, 013004 (2015).

[29] T. L. Gustavson, P. Bouyer, and M. A. Kasevich, Precision Rotation Measurements with an Atom Interferometer Gyroscope, Phys. Rev. Lett. **78**, 2046 (1997).

[30] H. Batelaan, E. M. Rasel, M. K. Oberthaler, J. Schmiedmayer, and A. Zeilinger, Anomalous transmission in atom optics, J. Mod. Opt. **44**, 2629 (1997).

[31] C. Garcion, N. Fabre, H. Bricha, F. Perales, S. Scheel, M. Ducloy, and G. Dutier, Intermediate-Range Casimir-Polder Interaction Probed by High-Order Slow Atom Diffraction, Phys. Rev. Lett. **127**, 170402 (2021).

[32] A. M. Wodtke, J. C. Tully, and D. J. Auerbach, Electronically non-adiabatic interactions of molecules at metal surfaces: Can we trust the Born–Oppenheimer approximation for surface chemistry? Int. Rev. Phys. Chem. **23**, 513 (2004).

[33] K. Golibrzuch, N. Bartels, D. J. Auerbach, and A. M. Wodtke, The dynamics of molecular interactions and chemical reactions at metal surfaces: Testing the foundations of theory, Annu. Rev. Phys. Chem. **66**, 399 (2015).

[34] S. Saxena and R. Joshi, *Thermal Accommodation and Adsorption Coefficients of Gases*, CINDAS data series on material properties, (Hemisphere, London, 1989).

[35] A. C. Dorst, F. Güthoff, D. Schauermann, A. M. Wodtke, D. R. Killelea, and T. Schäfer, Velocity map images of desorbing oxygen from sub-surface states of Rh(111), Phys. Chem. Chem. Phys. **24**, 26421 (2022).

[36] L. Lecroart, N. Hertl, Y. Dorenkamp, H. Jiang, T. N. Kitsopoulos, A. Kandratsenka, O. Bünermann, and A. M. Wodtke, Adsorbate modification of electronic nonadiabaticity: H atom scattering from $p(2\times2)$) O on Pt(111), J. Chem. Phys. **155**, 034702 (2021).

[37] J. Geweke and A. M. Wodtke, Vibrationally inelastic scattering of HCl from Ag(111), J. Chem. Phys. **153**, 164703 (2020).

[38] A. S. Palau, S. D. Eder, G. Bracco, and B. Holst, Neutral helium microscopy (SHeM): A review, arxiv:2111.12582.

[39] B. Holst and W. Allison, An atom-focusing mirror, Nature (London) **390**, 244 (1997).

[40] D. Barredo, F. Calleja, A. Weeks, P. Nieto, J. Hinarejos, G. Laurent, A. Vazquez de Parga, D. MacLaren, D. Farías, W. Allison, and R. Miranda, Si(111)–H(1×1): A mirror for atoms characterized by AFM, STM, He and H_2 diffraction, Surf. Sci. **601**, 24 (2007).

[41] J. R. Buckland and W. Allison, Determination of the helium/Si(111)–(1×1)H potential, J. Chem. Phys. **112**, 970 (2000).

[42] J. R. Buckland, B. Holst, and W. Allison, Helium reflectivity of the Si(111)-H(1 × 1) surface for use in atom optical elements, Chem. Phys. Lett. **303**, 107 (1999).

[43] D. A. MacLaren, N. J. Curson, P. Atkinson, and W. Allison, An AFM study of the processing of hydrogen passivated silicon(111) of a low miscut angle, Surf. Sci. **490**, 285 (2001).

[44] C. Brand, M. Sclafani, C. Knobloch, Y. Lilach, T. Juffmann, J. Kotakoski, C. Mangler, A. Winter, A. Turchanin, J. Meyer, O. Cheshnovsky, and M. Arndt, An atomically thin matter-wave beamsplitter, Nat. Nanotechnol. **10**, 845 (2015).

[45] C. Brand, F. Kiałka, S. Troyer, C. Knobloch, K. Simonović, B. A. Stickler, K. Hornberger, and M. Arndt, Bragg Diffraction of Large Organic Molecules, Phys. Rev. Lett. **125**, 033604 (2020).

[46] R. Brühl, P. Fouquet, R. E. Grisenti, J. P. Toennies, G. C. Hegerfeldt, T. Köhler, M. Stoll, and C. Walter, The van der Waals potential between metastable atoms and solidsurfaces: Novel diffraction experiments *vs.* theory, Europhys. Lett. **59**, 357 (2002).

[47] C. Kittel, *Introduction to Solid State Physics*, 8th ed., (Wiley, New York, 2004).

[48] A. S. Palau, S. D. Eder, T. Andersen, A. K. Ravn, G. Bracco, and B. Holst, Center-line intensity of a supersonic helium beam, Phys. Rev. A **98**, 063611 (2018).

[49] S. D. Eder, A. Salvador Palau, T. Kaltenbacher, G. Bracco, and B. Holst, Velocity distributions in microskimmer supersonic expansion helium beams: High precision measurements and modeling, Rev. Sci. Instrum. **89**, 113301 (2018).

[50] J. Fiedler, K. Berland, J. W. Borchert, R. W. Corkery, A. Eisfeld, D. Gelbwaser-Klimovsky, M. M. Greve, B. Holst, K. Jacobs, M. Krüger, D. F. Parsons, C. Persson, M. Presselt, T. Reisinger, S. Scheel, F. Stienkemeier, M. Tømterud, M. Walter, R. T. Weitz, and J. Zalieckas, Perspectives on weak interactions in complex materials at different length scales, Phys. Chem. Chem. Phys. **25**, 2671 (2023).

[51] H. Bender, C. Stehle, C. Zimmermann, S. Slama, J. Fiedler, S. Scheel, S. Y. Buhmann, and V. N. Marachevsky, Probing Atom-Surface Interactions by Diffraction of Bose-Einstein Condensates, Phys. Rev. X **4**, 011029 (2014).

[52] E. Galiffi, C. Sünderhauf, M. DeKieviet, and S. Wimberger, Two-dimensional simulation of quantum reflection, J. Phys. B: At., Mol. Opt. Phys. **50**, 095001 (2017).

[53] B. A. Stickler, U. Even, and K. Hornberger, Quantum reflection and interference of matter waves from periodically doped surfaces, Phys. Rev. A **91**, 013614 (2015).

[54] B. S. Zhao, S. A. Schulz, S. A. Meek, G. Meijer, and W. Schöllkopf, Quantum reflection of helium atom beams from a microstructured grating, Phys. Rev. A **78**, 010902(R) (2008).

[55] T. E. Judd, R. G. Scott, A. M. Martin, B. Kaczmarek, and T. M. Fromhold, Quantum reflection of ultracold atoms from thin films, graphene and semiconductor heterostructures, New J. Phys. **13**, 083020 (2011).

[56] L. Y. Kim, S. Park, C. Y. Lee, W. Schöllkopf, and B. S. Zhao, Enhanced elastic scattering of He_2 and He_3 from solids by multiple-edge diffraction, Phys. Chem. Chem. Phys. **24**, 21593 (2022).

[57] E. Bogomolny and C. Schmit, Asymptotic behaviour of multiple scattering on an infinite number of parallel half-planes, Nonlinearity **16**, 2035 (2003).